

Expression of symptoms elicited by a hammerhead viroid through RNA silencing is related to population bottlenecks in the infected host

Pedro Serra¹ , Beatriz Navarro² , Javier Forment¹ , Andreas Gisel^{3,4} , Selma Gago-Zachert⁵ ,
Francesco Di Serio²  and Ricardo Flores^{1†} 

¹Instituto de Biología Molecular y Celular de Plantas (Consejo Superior de Investigaciones Científicas–Universitat Politècnica de València), 46022 Valencia, Spain; ²Institute for Sustainable Plant Protection, National Research Council, Bari 70122, Italy; ³Institute for Biomedical Technologies, National Research Council, Bari 70122, Italy; ⁴International Institute of Tropical Agriculture, 200001 Ibadan, Nigeria; ⁵Section Microbial Biotechnology, Institute of Biochemistry and Biotechnology, Martin Luther University Halle-Wittenberg, 06120 Halle/Saale, Germany

Summary

Author for correspondence:
Francesco Di Serio
Email: francesco.diserio@ipsp.cnr.it

Received: 23 December 2022
Accepted: 16 March 2023

New Phytologist (2023)
doi: 10.1111/nph.18934

Key words: *Avsunviroidae*, chloroplastic transketolase, chrysanthemum chlorotic mottle viroid, noncoding RNA, pathogenesis, RNA silencing, superinfection exclusion.

- Chlorosis is frequently incited by viroids, small nonprotein-coding, circular RNAs replicating in nuclei (family *Pospiviroidae*) or chloroplasts (family *Avsunviroidae*). Here, we investigated how chrysanthemum chlorotic mottle viroid (CChMVd, *Avsunviroidae*) colonizes, evolves and initiates disease.
- Progeny variants of natural and mutated CChMVd sequence variants inoculated in chrysanthemum plants were characterized, and plant responses were assessed by molecular assays.
- We showed that: chlorotic mottle induced by CChMVd reflects the spatial distribution and evolutionary behaviour in the infected host of pathogenic (containing a UUUC tetranucleotide) and nonpathogenic (lacking such a pathogenic determinant) variants; and RNA silencing is involved in the initiation of the chlorosis in symptomatic leaf sectors through a viroid-derived small RNA containing the pathogenic determinant that directs AGO1-mediated cleavage of the mRNA encoding the chloroplastic transketolase.
- This study provides the first evidence that colonization of leaf tissues by CChMVd is characterized by segregating variant populations differing in pathogenicity and with the ability to colonize leaf sectors (bottlenecks) and exclude other variants (superinfection exclusion). Importantly, no specific pathogenic viroid variants were found in the chlorotic spots caused by chrysanthemum stunt viroid (*Pospiviroidae*), thus establishing a clear distinction on how members of the two viroid families trigger chlorosis in the same host.

Introduction

Viroids are the smallest RNAs replicons endowed with autonomous replication (Diener, 2003; Steger & Riesner, 2018). Whereas viruses require that the proteins they encode interact with some factors from the host for replication and movement, viroid genomes – composed of a nonprotein-coding single-stranded circular RNA of only 250–430 nucleotides (nt) – contain all the information needed to manipulate the RNA transcription, processing and trafficking machinery of their hosts, in which they may cause a disease (Ding, 2009; Kovalskaya & Hammond, 2014; Wang *et al.*, 2018; Adkar-Purushothama & Perreault, 2020; Wu *et al.*, 2020; Navarro *et al.*, 2021a). Viroids are classified into two families. Those clustered in the *Pospiviroidae* (Di Serio *et al.*, 2021), type member potato spindle tuber

viroid (PSTVd) (Diener, 1971; Gross *et al.*, 1978), have a central conserved region (CCR) (McInnes & Symons, 1991), do not contain hammerhead ribozymes, and replicate in the nucleus through an asymmetric RNA–RNA rolling-circle mechanism. On the contrary, those grouped in the *Avsunviroidae* (Di Serio *et al.*, 2018), type member avocado sunblotch viroid (ASBVd) (Symons, 1981; Hutchins *et al.*, 1986), lack a CCR. However, embedded in their strands of either polarity, members of this viroid family have hammerhead ribozymes that mediate co-transcriptional self-cleavage of the oligomeric RNAs generated during replication in plastids (mostly chloroplasts) through a symmetric RNA–RNA rolling-circle mechanism (Navarro *et al.*, 2021a).

Viroid-derived small RNAs (vd-sRNAs) resembling the small interfering RNAs (siRNAs) and microRNAs (miRNAs; Papaefthimiou *et al.*, 2001; Martínez de Alba *et al.*, 2002) have been detected in plants infected by members of the two families. These findings, combined with the observation that partial-length

†This paper is dedicated to the memory of our mentor, colleague and friend Professor Ricardo Flores.

inverted repeats of PSTVd transgenically expressed in tomato elicit viroid-like symptoms and accumulate PSTVd-sRNAs, have led to deem that vd-sRNAs might target host mRNAs for inactivation via RNA silencing (Wang *et al.*, 2004). In this context, vd-sRNAs would bind and guide Argonaute (AGO) proteins, at the core of the RNA inducing silencing complex (RISC), to inactivate complementary DNA or RNA resulting in transcriptional or post-transcriptional gene silencing, respectively (Mallory & Vaucheret, 2010; Poulsen *et al.*, 2013; Fang & Qi, 2016; Ma & Zhang, 2018). There is direct evidence that PSTVd-sRNAs bind *in vivo* several AGOs (Minoia *et al.*, 2014), including AGO1 that has a clear preference for 21–22-nt sRNAs with a 5'-terminal U (Mi *et al.*, 2008; Montgomery *et al.*, 2008). More specifically, the idea that the primary molecular lesion inducing peach calico (PC, albinism) and peach yellow mosaic (PYM) is triggered by vd-sRNAs containing the pathogenic determinants of some variants of peach latent mosaic viroid (PLMVd, genus *Pelamoviroid* within the *Avsunviroidae*, Hernández & Flores, 1992) has received sound support (Navarro *et al.*, 2012; Delgado *et al.*, 2019). These PLMVd-sRNAs target for cleavage, at the sites predicted by RISC(AGO1)-mediated RNA silencing, the mRNAs coding for proteins implicated in chloroplast biogenesis/function, thus eliciting the initial lesions eventually resulting in specific chloroses.

In this framework, the system formed by another pelamoviroid, chrysanthemum chlorotic mottle (CChMVd; Navarro & Flores, 1997), infecting chrysanthemum offers important advantages. The herbaceous nature of the host allows a more precise capture of the viroid variants associated with early symptoms (10–12 d) than in the PLMVd-peach system (wherein onset of symptoms usually takes 1.5–2 months). Moreover, the pathogenic determinant of CChMVd has been mapped at a tetraloop within a branched conformation (de la Peña *et al.*, 1999), with the existence of a similar secondary structure similar to PLMVd, stabilized by a kissing-loop interaction predicted *in silico* (Busière *et al.*, 2000), supported by chemical probing *in vitro* (Giguère *et al.*, 2014) and by co-variation analyses *in vivo* (de la Peña *et al.*, 1999; de la Peña & Flores, 2002; Gago *et al.*, 2005). In addition, the mutation rate of CChMVd has been determined and found to be one of the highest reported for any biological entity (Gago *et al.*, 2009). As a disadvantage, the chrysanthemum genome is complex (hexaploid) and poorly annotated. Despite this limitation, CChMVd, which induces the accumulation of abundant vd-sRNAs in chrysanthemum (Martínez de Alba *et al.*, 2002), provides an excellent opportunity to test and get a deeper insight into how viroids colonize, evolve and initiate disease in their hosts.

Here, we show that during host infection, CChMVd (*Avsunviroidae*) displays a 'territorial behavior' resulting in segregated populations most likely derived from the concerted effects of the extremely high mutation rate of this viroid and the ability of some of its variants to colonize leaf sectors (via bottlenecks) and exclude other variants (by superinfection exclusion). Therefore, we provide the first evidence of the role of bottleneck and superinfection exclusion dynamics in viroid evolution during host colonization. Moreover, our data support that the chlorotic

mottle induced by the viroid is initiated by a 21-nt vd-sRNA containing most of the pathogenic UUUC sequence, which primes RISC(AGO1)-mediated cleavage of the mRNA encoding the chloroplastic transketolase. Remarkably, a similar mechanism does not operate in triggering the chlorotic spots incited by chrysanthemum stunt viroid (CSVd, *Pospiviroidae*), thus setting a clear difference on how members of both viroid families initiate disease in a common host.

Materials and Methods

Plant material and bioassays

All trials in this study were conducted with chrysanthemum (*Dendranthema grandiflora* Tzvelev, syn. *Chrysanthemum morifolium* Ramat, 'Bonnie Jean' plants vegetatively propagated and mechanically inoculated in the three upper leaves with viroid RNA variants (40 ng per leaf) generated by *in vitro* transcription as reported (Gago *et al.*, 2005). The primary transcripts of head-to-tail dimeric constructs were separated by denaturing (1× TBE and 8 M urea) 5% PAGE and the self-cleaved CChMVd monomeric RNAs and the CSVd dimeric RNAs (ID: AB679193) were eluted and quantified. Inoculated plants were maintained in a glasshouse at a constant temperature of 28°C and a photoperiod of 18-h : 6-h, light : dark. Chlorotic and green sectors were separately sampled and extracted from expanded leaves (longitudinal size of the mid rib 5–6 cm). In the case of leaves infected with CSVd, which generally induces smaller chlorotic areas than CChMVd, sampling was carried out using a borer consisting of a plastic tip. When needed, the plastic tip was transversally cut to have an appropriate diameter covering an area smaller than the chlorotic lesion to be collected, thus excluding the surrounding green tissue. In the case of chlorotic lesions with a diameter of < 3 mm, the samples were collected using a magnifying glass.

RNA extraction, Northern blot assays and characterization of viroid progeny variants

Total RNA was extracted with TRIzol (Invitrogen) from 100 mg of leaves, resuspended in 100 µl, treated with 2 U of Turbo DNase (Invitrogen) and quantified with a 2100 Bioanalyzer Instrument (Agilent, Santa Clara, CA, USA). For Northern blot hybridization, viroid-enriched RNA preparations were obtained from leaves (1 g) by phenol extraction followed by chromatography on nonionic cellulose (CF-11; Whatman, Maidstone, UK) (Gago *et al.*, 2005), separated in nondenaturing (1× TAE) or denaturing (1× TBE and 8 M urea) 5% PAGE, electroblotted to positively charged nylon membranes (Roche) and hybridized with specific digoxigenin-labelled riboprobe as reported (Navarro *et al.*, 2021b). To characterize the progeny variants, viroid-enriched RNA preparations were reverse-transcribed with Superscript II reverse transcriptase following the supplier (Invitrogen) protocol. The resulting cDNAs were amplified with Pfu DNA polymerase (Agilent) by 30 amplification cycles (95°C for 30 s, 60°C for 30 s and 72°C for 40 s) using specific primers (Supporting Information Table S1).

Amplification products of the expected size were cloned and sequenced with an ABI 3100 Genetic Analyzer (Applied Biosystems, Waltham, MA, USA).

Site-directed mutagenesis, construction of CChMVd dimeric cDNA clones and *in vitro* transcription

The mutant plasmid pCM20-U89mut was generated by site-directed mutagenesis from a plasmid containing the full-length sequence of CChMVd CM20 variant, following a PCR-based protocol reported previously (Gago *et al.*, 2005) and using primers RF-1425 and RF-1424 (Table S1). Head-to-tail dimeric cDNA constructs of natural and mutated CChMVd variants were obtained by ligation with T4 DNA ligase of the respective monomeric cDNAs amplified by PCR from the appropriate plasmids using the primers RF-959 and RF-958 (Table S1) and Pfu DNA polymerase (Agilent). The resultant dimeric molecules were cloned and sequenced.

Transcriptome and sRNAs sequencing and bioinformatics analyses

Total RNA preparation treated with Turbo DNase (see above) were used to generate RNA-Seq libraries using TruSeq Stranded mRNA Sample Preparation kit (Illumina, San Diego, CA, USA) and sequenced (2 × 150 bp paired-end) on the HiSeq 4000 system (Fasteris, Geneva, Switzerland). After adapter trimming, *de novo* assembly was performed using VELVET v.1.2.10 (Zerbino & Birney, 2008) and OASES v.0.2.08 (Schulz *et al.*, 2012), and the obtained contigs were used to identify the sequences of the gene of interest by BLASTN, BLASTX and searches in the recently released *C. morifolium* genome (<http://210.22.121.250:8880/asteraceae/browse/genomePage/Cmo>).

cDNA libraries of sRNAs (16–30 nt) were generated and sequenced (1 × 50 bp) on an Illumina Genome HiSeq 2500 Analyzer (Fasteris). After trimming and filtering by quality control, the reads were mapped to CChMVd sequence variants with an in-house pipeline (Navarro *et al.*, 2012). Putative mRNAs targeted by vd-sRNAs were searched using psRNATarget program (Dai *et al.*, 2018) on the FASTA collection of chrysanthemum RNA contigs. Chloroplastic transit peptides in the encoded proteins were predicted by CHLOROP (Emanuelsson *et al.*, 1999). Sequence alignments were carried out with CLUSTAL OMEGA (Sievers & Higgins, 2014).

5' RNA ligase-mediated rapid amplification of cDNA ends (RLM-RACE)

RLM-RACE were performed as reported previously (Delgado *et al.*, 2019). Briefly, an RNA adaptor (5'-CGACUGGAGCAC GAGGACACUGACAUGGACUGAAGGAGUAGAAA-3') was ligated to DNA-free total RNA and used for cDNA synthesis using the primer RF-3400 (complementary to TKT mRNA) that was amplified by a first PCR, using the primers RF-3400 and RF-553 (homologous to the RNA adaptor). The expected product of *c.* 242 bp was gel purified and subjected to a second

(nested) PCR with primers RF-3402 (internal with respect to RF-3400) and RF-554 (internal with respect to RF-553). The expected product of *c.* 196 bp was eluted, cloned and sequenced.

Quantification of mRNA accumulation by RT-qPCR

Aliquots (2.5 µl) of DNA-free total RNA preparations were reverse transcribed (RT) with Superscript II (Invitrogen) and random hexanucleotides as reported previously (Delgado *et al.*, 2019). Aliquots (1 µl) of the RT reaction were used to perform qPCR with specific primers (Table S1 and Dataset S1) and SYBR green PCR master mix following supplier instructions (Applied Biosystems). Amplification efficiency of all primers was between 90% and 110%, with R^2 -value between 0.98 and 1. Each qPCR was repeated at least in triplicate on three biological replicates. Controls without template were included for each primer pair. C_t values were used to analyse relative gene expression in symptomatic and nonsymptomatic sectors of the same CChMVd-infected leaves and in leaves from mock-inoculated plants. The relative expression level of the selected transcripts was calculated by the $2^{-\Delta\Delta C_t}$ method (Livak & Schmittgen, 2001) using the elongation factor 1 α (EF1 α) as the internal reference gene. Relative quantification data were subjected to a logarithm transformation to resemble a normal distribution, and statistical significance was assessed by One-way ANOVA with Duncan's multiple-range test for comparison between groups (Bewick *et al.*, 2004). Statistical analyses were performed using the STATGRAPHICS CENTURION software.

Protein extraction and Western blot

Total proteins were extracted with 100 mM Tris-HCl, pH 6.8, containing 0.3% β -mercaptoethanol and 1 mM phenylmethyl-sulfonyl fluoride from 1 g of leaves. Aliquots of protein preparations were subjected to 12% SDS-PAGE, transferred to polyvinylidene difluoride (PVDF) membranes (Roche), and immunoblotted with antisera against transketolase (chloroplastic; anti-TKL-1; Agrisera, Vännäs, Sweden) at a 1 : 5000 dilution. Goat antirabbit horseradish peroxidase (HRP) conjugated (Agrisera) at a 1 : 10 000 dilution was used as secondary antibody, and immunoreactive bands were revealed with the chemiluminescence ECL Plus kit, following supplier recommendations (GE Healthcare, Chicago, IL, USA). Signals were recorded by autoradiography.

Results

CChMVd symptomatic and nonsymptomatic variants behave differently during host colonization

To learn how CChMVd colonizes, evolves and incites disease in its natural/experimental host (chrysanthemum), two viroid variants, one with a UUUC tetraloop strictly associated with symptoms and the other nonsymptomatic and just differing in an alternative GAAA tetraloop (Fig. 1; de la Peña *et al.*, 1999; de la Peña & Flores, 2002), were assayed. Upper noninoculated leaves

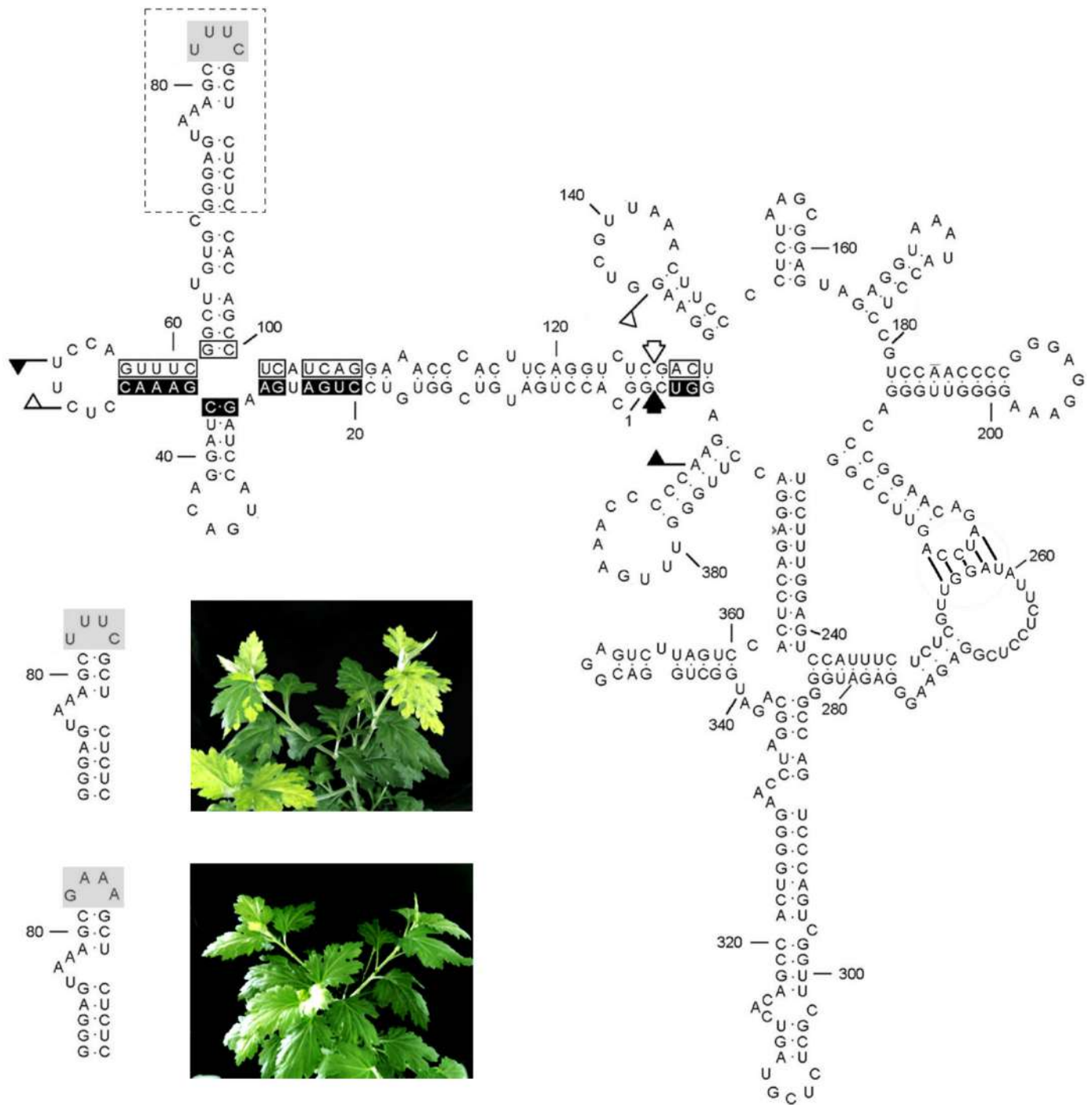


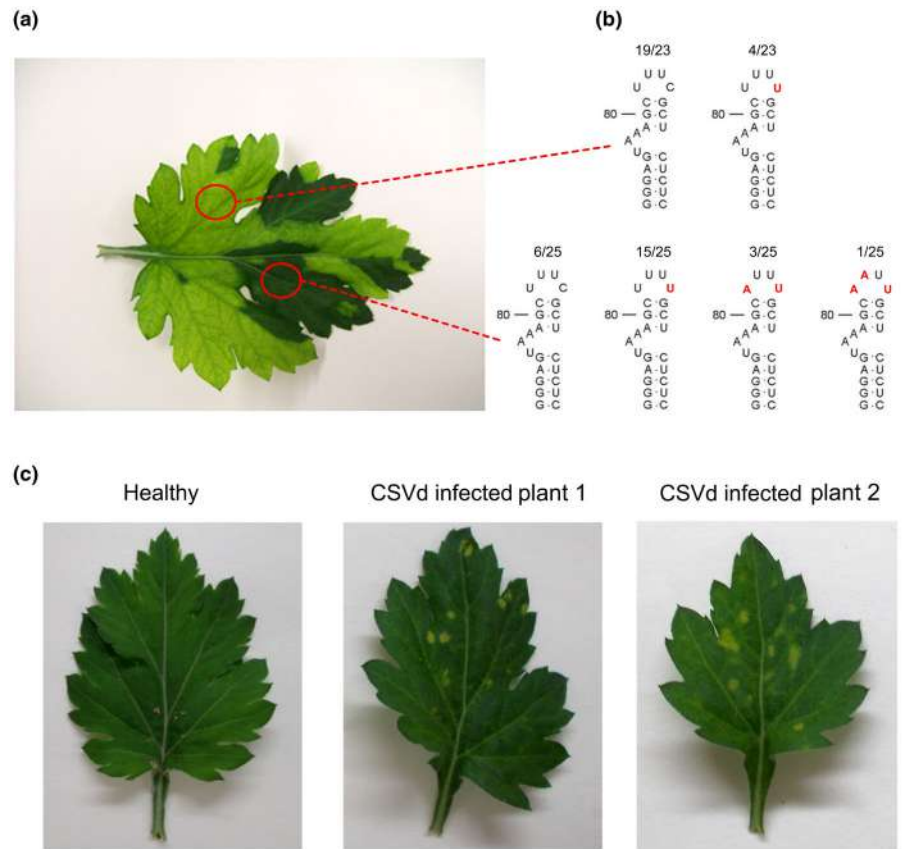
Fig. 1 Branched conformation adopted by chrysanthemum chlorotic mottle viroid (variant CM20, ID AJ878085). Plus (open symbols) and minus (close symbols) self-cleaving domains are delimited by flags, residues conserved in most natural hammerhead structures are indicated by boxes, and the self-cleavage sites are marked by arrows. Residues between nucleotides at positions 220–224 and 255–259 involved in a kissing loop interaction stabilizing the viroid conformation are indicated by lines. The UUUC tetraloop (positions 82–85), which was identified as the pathogenic determinant of CChMVd, is on a gray background. The dotted line box indicates the hairpin containing the tetraloop shown in the inset (up). The variants in which the pathogenic determinant is replaced by a GAAA tetraloop (inset, down) do not induce leaf symptoms in chrysanthemum.

were collected 20-d postinoculation (dpi) to characterize the infecting viroid population.

As expected, the variant with the GAAA tetraloop induced no phenotype, while the variant with the UUUC tetraloop (the

pathogenic determinant; CChMVd-S) induced early symptoms consisting in adjacent chlorotic and green leaf sectors (Fig. 2a). Moreover, RT-PCR, cloning and sequencing showed that the progeny of the variant with the GAAA tetraloop (IDs from

Fig. 2 Symptoms induced by the pathogenic CChMVd variant (CM20) in chrysanthemum leaves (a). The viroid progeny was characterized by cloning and sequencing viroid full-length cDNAs generated by RT-PCR using RNA preparations extracted from adjacent chlorotic and green sectors (red circles) of symptomatic leaves. The hairpin sequences containing the pathogenic determinant (UUUC tetraloop) or a mutated loop found in the progenies are reported, with the fractions on the top indicating the number of clones containing each reported variant from the symptomatic (upper; IDs from OP918681 to OP918703) and nonsymptomatic (lower; IDs from OP918704 to OP918728) leaf sectors (b). Symptoms induced on leaves (longitudinal size of the mid rib 5–6 cm) in chrysanthemum 'Bonnie Jean' by CSVd (c).



OP918729 to OP918758) consisted of most variants (28 of 30) presenting the same GAAA tetraloop, with the remaining having one single mutation, either UAAA (one of 30; ID: OP918740) or AAAA (one of 30; ID: OP918743). The progeny of the CChMVd-S variant differed in chlorotic and green sectors: variants with the UUUC tetraloop predominated in chlorotic sectors (19 of 23), together with minor proportions of others with one substitution (generating the tetraloop UUUU; Fig. 2b); by contrast, in green sectors, the ratio of UUUC variants was low (six of 25) and they coexisted with others harbouring one (UUUU), two (AUUU) or three (AAUU) substitutions in the pathogenic determinant (Fig. 2b). Interestingly, Northern blot hybridization assays showed that the viroid accumulated at similar levels in both symptomatic and green sectors (Fig. S1).

Bioassays of the three latent variants (with a tetraloop UUUU, AUUU and AAUU) resulted in nonsymptomatic infections (at 20 dpi), revealing that one single substitution in this tetraloop annuls pathogenicity (Fig. S2). The UUUC tetraloop was not found in the progeny variants of the mutants with the AUUU or AAUU tetraloop, although other nucleotide changes were observed (Fig. S2). However, a minor proportion (two of 12) of variants with UUUC tetraloop was detected in the progeny of the mutant containing the UUUU tetraloop. In one of the plants inoculated with this variant, a small chlorotic sector was observed at a late infection stage (4-wk postinoculation) and, remarkably, the UUUC tetraloop reappeared in nine of 10 progeny variants from the symptomatic tissue (Fig. S2). Hence, symptomatic and

nonsymptomatic CChMVd variants (hereafter denoted as CChMVd-S and CChMVd-NS, respectively) follow distinct evolutionary trajectories, with the latter prevalently evolving from the former. The other way around, evolution from nonsymptomatic to symptomatic CChMVd variants, is less frequent and limited only to the inoculated variants containing a UUUU tetraloop. CChMVd thus shows a 'territorial behavior', with clearly segregated populations in a single leaf. The finding that a single substitution in the UUUC tetraloop disrupts pathogenicity is consistent with the involvement of RNA silencing in initiating the disease (see below).

To better assess these conclusions, we performed two additional experiments. In the first one, we inoculated the CChMVd-S variant CM20 (with the UUUC tetraloop) and just 5 dpi examined the progeny in upper noninoculated young leaves. All variants recovered (12 of 12) did not show changes in the tetraloop (Fig. S3). This result suggests that 5 dpi chrysanthemum plants become systemically infected by variants containing the pathogenic determinant. However, longer time intervals are needed for the emergence of the variants with mutations in this tetraloop shown in a previous experiment to preferentially accumulate in green sectors of symptomatic leaves at 20 dpi (Fig. 2a). In addition, symptom expression and sectorization of chlorotic tissues may require an appropriate leaf developmental stage and/or a minimum accumulation level of pathogenic variants in the infected tissues and/or a certain time for the plant defence responses to initiate the pathogenic process. Indeed, at this early

stage (5 dpi), tissues infected by variants containing the pathogenic UUUC tetraloops did not show chlorosis.

In the second experiment, we turned our attention to the well-defined chlorotic leaf spots induced in the same host (chrysanthemum 'Bonnie Jean') by a nuclear-replicating viroid (chrysanthemum stunt viroid, CSVd; Lawson, 1987; Fig. 2c). The accumulation level (Fig. S1) and, particularly, the sequence of the variants retrieved from both the yellow spots and the surrounding green tissue in CSVd infected plants did not show significant differences. In two sets of 20 sequence variants (10 from each type of tissue, and each set obtained with a pair of adjacent primers), only five showed a single point mutation, probably generated during the RT-PCR amplification (Fig. S4). Thus, in sharp contrast with the situation found for CChMVd, the CSVd-incited chlorosis is not associated with specific viroid variants, most likely because it does not represent a primary lesion but an intermediate/late symptom (see below).

CChMVd-sRNAs with the pathogenic determinant accumulate predominantly in chlorotic sectors

Considering the uneven distribution of CChMVd variants between chlorotic and green tissues of the same leaves, we anticipated a similar distribution for CChMVd-sRNAs with and without the intact pathogenic determinant, respectively. To gather evidence supporting this view, we generated four sRNA libraries from symptomatic and nonsymptomatic sectors of two leaves from chrysanthemum plants inoculated with the CChMVd pathogenic variant (CM20). For each sample, we obtained from *c.* 8 to 13 million reads of 18–26 nt, which showed a similar size distribution with two major peaks of 21 and 24 nt (Fig. S5; Table S2). CChMVd-sRNAs matching perfectly, or with one mismatch, the infecting variant or its progeny represented 12.4–15.7% in the chlorotic sectors and 10.6–10.7% in the green sectors (Table S2), thus confirming previous data from RNA gel-blot hybridization indicating that CChMVd is heavily targeted by the RNA silencing defensive response of its host (Martínez de Alba *et al.*, 2002).

Regarding size distribution of the CChMVd-sRNAs, the 21-nt species clearly predominated (*c.* 70%), with those from either polarity strands accumulating at similar rates (Fig. S5). The CChMVd-sRNAs from the four libraries spanned the whole genomic strands, with a coverage mean depth of 220–225 (Fig. S5), thus attesting to the reproducibility of the results.

The 21-nt CChMVd-sRNAs of either polarity strand containing the pathogenic determinant (positions 82–85; de la Peña *et al.*, 1999; de la Peña & Flores, 2002), accounted for 0.6–0.9% of the total viroid-derived reads in the four samples. More specifically, 90% of CChMVd 21-nt reads from the yellow sectors had the pathogenic determinant UUUC, whereas the rate was much lower (56% and 17%) in the green sectors (Table S3). When the nucleotide variability in the pathogenic determinant was assessed considering this subset of CChMVd-sRNAs, mutations were detected in all positions of the tetraloop, being the most abundant mutation C85 to U (Table S3). This mutated tetraloop (UUUU) only represented 7–8% in the reads from the yellow

sectors, while it was predominant (40–70%) in the green sectors (Table S3). These results were congruent with data obtained by cloning and conventional sequencing of the CChMVd progeny from both kind of leaf sectors (Fig. 2).

A quest of CChMVd-sRNAs with the pathogenic determinant unveils candidate targets in the chrysanthemum transcriptome

Because the complete chrysanthemum genome was not available, to search for potential targets of CChMVd-sRNAs containing the pathogenic determinant, a transcriptome was assembled *de novo* using mRNASeq data from a library generated from a non-infected chrysanthemum plant of cultivar 'Bonnie Jean'. A FASTA collection of 584 917 contigs, with an average length of 496 bases and a N50 value of 1151, was generated. The psRNATarget program (Dai *et al.*, 2018) was used to search for chrysanthemum transcripts potentially targeted for inactivation, via RNA silencing, by (+) vd-sRNAs containing the CChMVd pathogenic determinant (UUUC; or part of it) and by (–) vd-sRNAs containing the complementary sequence. We limited our search to 21-nt sRNAs, since this is the size of most CChMVd-sRNAs (Fig. S5) and plant miRNAs (Rogers & Chen, 2013). For finding vd-sRNA candidate targets, a cut-off score threshold of ≤ 2.5 , which is more stringent than the default parameters of psRNA-Target program (expectation ≤ 3) was adopted. This cut-off has been successfully used previously for identifying peach transcripts targeted by PLMVd-sRNAs initiating PYM (Delgado *et al.*, 2019). Additionally, another restriction was applied: the CChMVd-sRNA should have a 5'-terminal U, as those initiating PC and PYM do (Navarro *et al.*, 2012; Delgado *et al.*, 2019).

Following this approach, eight CChMVd-sRNAs, six of (+) and two of (–) polarity targeting eight chrysanthemum transcripts for potential RNA silencing-mediated degradation were identified (Table 1). Of these CChMVd-sRNAs, we focussed on CChMVd-sRNA3, of (+) polarity, which potentially targets an mRNA encoding a protein containing a chloroplastic transit peptide according to predictions with CHLOROP1.1 software (Table 1). CChMVd-sRNA3 is the only one having two terminal Us. Thus, it resembles the PLMVd-sRNAs initiating PC and PYM in peach (Navarro *et al.*, 2012; Delgado *et al.*, 2019); and the sRNA derived from a satellite RNA initiating a yellow mosaic on tobacco (Shimura *et al.*, 2011; Smith *et al.*, 2011; see the Discussion section), which at least have two 5'-terminal Us, strongly supporting the involvement of RISC(AGO1) given that AGO1 recruits preferentially sRNAs with such 5'-termini (Mi *et al.*, 2008; Montgomery *et al.*, 2008; Minoia *et al.*, 2014). There are additional reasons supporting this selection. First, the predominant mutation in the pathogenic determinant (UUUC to UUUU in the CChMVd genomic RNA) that abolishes pathogenicity (Figs 1, S2), maps at the third position of the CChMVd-sRNA3 (counting from its 5'-end), position in which mismatches, bulges or G:U pairs in the hybrids formed by miRNAs and their targets are barely or not tolerated at all (Fahlgren & Carrington, 2010). Second, the reads per million of CChMVd-sRNA3 were at least 10-fold higher in the chlorotic than in the green sectors (Table 1). And third, the

Table 1 Predicted chrysanthemum mRNA targets of CChMVd-sRNAs containing the pathogenic determinant.

sRNA ^a	sRNA 5'end ^b	Viroid strand ^c	RPM ^d	mRNA target:sRNA duplex ^e	mfe ^f	Score ^g	Target predicted function ^h	Chloroplast localization ⁱ
CChMVd-sRNA2	84	(+)	1.8/1.4//0.5/0.1	UUGACGCGUGGAGAAAGCGA : : : : : : : : : : : : : : : UACUCCGACACCUCUCGCGU	-35.7	2.5	Transketolase, chloroplastic	Yes
CChMVd-sRNA3	83	(+)	4/3.9//0.4/0.2	UGACGCGUGGAGAAAGCGAA : : : : : : : : : : : : : : : ACUCCGACACCUCUCGCGU	-35.8	2.5	Transketolase, chloroplastic	Yes
CChMVd-sRNA10	76	(+)	4.3/2.1//0/0	UCGGAGAGAUUGAAAGCUUUA : : : : : : : : : : : : : : : CACCCUCUCGCGUUUCGAAAU	-32.2	2.0	Ferric reduction oxidase 4-like	No
CChMVd-sRNA18	68	(+)	0.1/0//0/0	CGUGGAGCUUACUCGCCGGA : : : : : : : : : : : : : : : UCGCUUUCGAAAUAGAGGGCGU	-37	2.5	Probable pectinesterase/ pectinesterase inhibitor 34	No
CChMVd-sRNA20	66	(+)	16.8/20.7//7.8/5.9	UGGAAGCUUACUCGCCGACA : : : : : : : : : : : : : : : GCUUUCGAAAUAGAGGGCGU	-37.9	2.0	Probable pectinesterase/ pectinesterase inhibitor 34	No
CChMVd-sRNA20	66	(+)	16.8/20.7//7.8/5.9	AAAAACCUUUGUUUCCGCACA : : : : : : : : : : : : : : : GCUUUCGAAAUAGAGGGCGU	-24.2	2.5	ABC transporter E family member 2	No
CChMVd-sRNA21	65	(+)	39.8/45.2//18.3/10.8	UGAGACUUUAUCCUGCACAA : : : : : : : : : : : : : : : CUUUCGAAAUAGAGGGCGUU	-32.1	2.5	Disease resistance protein	No
CChMVd-sRNA21	65	(+)	39.8/45.2//18.3/10.8	GGAAGCUUACUCGCCGACAG : : : : : : : : : : : : : : : CUUUCGAAAUAGAGGGCGUU	-36.6	2.0	Probable pectinesterase/ pectinesterase inhibitor 34	No
CChMVd-sRNA24	103	(-)	79.5/76.3//24.6/15.5	UUUGCUCUCUCACAGUCUCG : : : : : : : : : : : : : : : AAGCGAGAGGUGUCGGAGU	-40.1	2.0	Cysteine proteinase RD21A- like	No
CChMVd-sRNA32	95	(-)	0.4/0.4//0.1/0.2	UUAAAGAUUUUGCUUUCUCA : : : : : : : : : : : : : : : CAUUUCGAAAGCGAGAGAGGU	-26.9	2.5	U-box domain-containing protein 17-like	No
CChMVd-sRNA32	95	(-)	0.4/0.4//0.1/0.2	UCAAAGUUUUUGCUUUCUCA : : : : : : : : : : : : : : : CAUUUCGAAAGCGAGAGAGGU	-28.1	2.5	Ubiquitin-conjugating enzyme E2	No

^aCChMVd-small RNAs with 5' terminal U and containing at least one nucleotide of the pathogenic determinant.

^bPosition of the CChMVd-sRNA 5' termini in the genomic RNA of CChMVd variant CM20.

^c(+) and (-) indicate plus and minus sRNA polarity, respectively.

^dReads per million (RPM) of the vd-sRNA in symptomatic//non-symptomatic sectors (two samples).

^emRNA:CChMVd-sRNA duplexes predicted by psRNATarget (Dai *et al.*, 2018); host targeted mRNAs on top (5'-3' orientation) and CChMVd-sRNAs are on the bottom (3'-5' orientation). Nucleotides spanning the CChMVd pathogenic determinant are in bold; (:) Watson-Crick base pairs; (.) G : U wobble base pairs.

^fMinimum free energy (kcal mol⁻¹) of the vd-sRNA:mRNA target duplex predicted by RNA hybrid (Rehmsmeier *et al.*, 2004).

^gScore of the mRNA target:sRNA duplex, estimated by psRNATarget (Dai *et al.*, 2018); the lower the score, the more reliable the prediction.

^hTarget function predicted by sequence homology.

ⁱChloroplast targeting of the protein predicted by CHLORO-P software (<http://www.cbs.dtu.dk/services/ChloroP>).

predicted chrysanthemum target of CChMVd-sRNA3 codes for a protein of 743 amino acids displaying high identity (82.51%) with the chloroplastic transketolase (TKT) of *Arabidopsis* (NP_567103.1) and of other plants (Fig. 3), a nuclear-encoded protein that, when silenced transgenically in tobacco (Henkes *et al.*, 2001) or via virus-induced gene silencing in *Nicotiana benthamiana* (Yuan *et al.*, 2011), results in chlorotic phenotypes resembling that incited by CChMVd. These data, collectively, supported that CChMVd-sRNA3 may downregulate the expression of the *TKT* gene by directing cleavage of its mRNA.

A CChMVd-sRNA with the pathogenic determinant targets for RISC(AGO1)-mediated cleavage the mRNA of the chloroplastic TKT and reduces its protein levels

To test whether CChMVd-sRNA3 guides RISC(AGO1)-mediated cleavage of the TKT mRNA, an RNA ligase-mediated rapid amplification of 5'-cDNA ends (RLM-RACE) protocol

was applied to two RNA preparations from chlorotic and green sectors of the same chrysanthemum leaf. An amplification product of expected size was obtained only from chlorotic sectors. Sequencing of the cloned amplification products from the symptomatic tissues showed that 15/15 clones indeed derived from the TKT transcript and had the 5' termini predicted considering the CChMVd-sRNA3-guided cleavage: between positions 10 and 11 counting from its 5' terminus (Fig. 4). This result also discards RISC(AGO1)-mediated cleavage of the TKT mRNA by the other candidate, CChMVd-sRNA2, because the cleavage site guided by CChMVd-sRNA2 would be displaced one position from the canonical site (Table 1). In addition, the involvement of a CChMVd-sRNA identical to CChMVd-sRNA3 but with an extra 5'-U and, therefore of 22 nt, seems also unlikely because the extra nucleotide does not form a canonical base-pair in the predicted hybrid and the predicted cleavage site in the TKT transcript is displaced one position. Altogether such data strongly support our working hypothesis: TKT mRNA cleavage primed



Fig. 3 Multiple alignment of chloroplast transketolase (TKT) proteins encoded by the genomes of *Chrysanthemum morifolium* Ramat (Cm), *Artemisia annua* L. (Aa), *Helianthus annuus* L. (Ha), *Nicotiana benthamiana* Domin (Nb), *Nicotiana tabacum* L. (Nt), *Arabidopsis thaliana* (L.) Heynh. (At), and *Oryza sativa* L. (Os). Positions in the TKTs are reported on the right. In red, hydrophobic amino acids (aa) (AVPMIL) and the aromatic F and W; in blue, acidic aa (DE); in magenta, basic aa (RK) except H; in green, polar aa (CSTNQ and Y), H and G. The arrow on the top indicates the C-terminal amino-acid of the chloroplast transit peptide predicted by the CHLORO-P Program (Emanuelsson *et al.*, 1999).

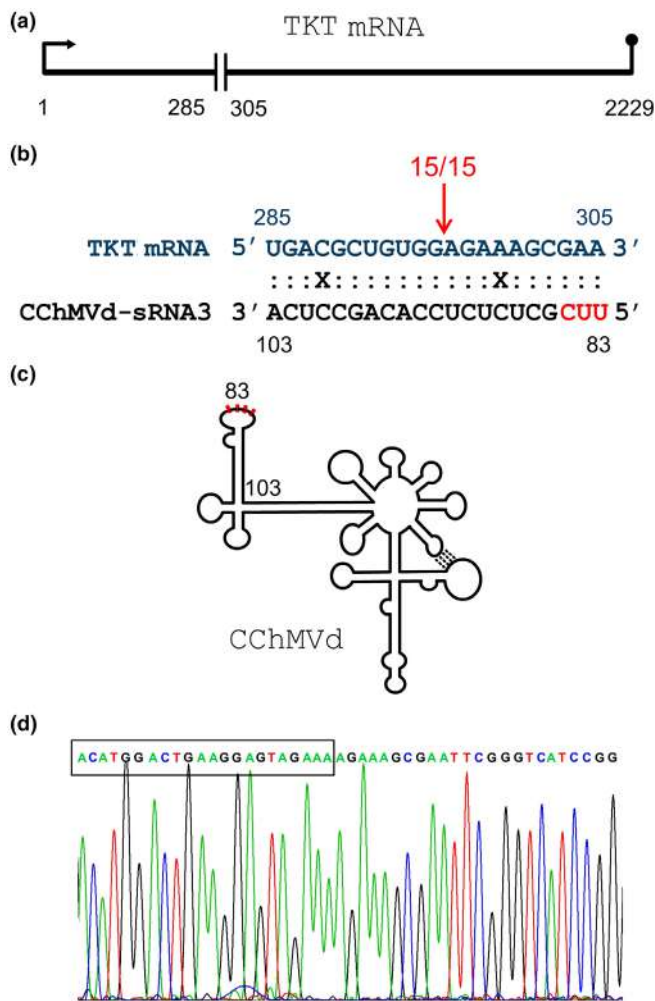


Fig. 4 Site-specific cleavage of the chrysanthemum transketolase (TKT) mRNA through RNA silencing machinery guided by CChMVd-sRNA3. Targeted region within the TKT mRNA (a). Hybrid formed by CChMVd-sRNA3 and the targeted TKT mRNAs sequence (with CChMVd-sRNA3 nucleotides containing the pathogenic motif reported in red and the expected cleavage site marked by the red arrow; all sequenced clones (15/15 in red) of the 5' RNA ligase-mediated rapid amplification of cDNA ends (RLM-RACE) amplification products from the symptomatic tissues confirmed the predicted cleavage site (b). Position of the pathogenic motif (UUUC, in red) in the viroid secondary structure (c). Sequencing electropherogram of RLM-RACE products obtained from symptomatic tissues (RNA adaptor is boxed) (d).

by CChMVd-sRNA3 takes place predominantly in the chlorotic sectors, where the latter accumulates preferentially.

It has been previously shown that in viroid-infected tissues the mRNAs targeted by vd-sRNAs-mediated cleavage may not necessarily accumulate at lower levels than in noninfected controls (Navarro *et al.*, 2021b). Therefore, we estimated by reverse transcription-quantitative polymerase chain reaction (RT-qPCR) the accumulation of the TKT and three other control mRNAs in chlorotic and green sectors from the same leaf, as well as from a leaf of a mock-inoculated plant. Whereas no significant changes were observed between the green leaf tissues from the CChMVd-infected and the mock-inoculated plants, significant differences

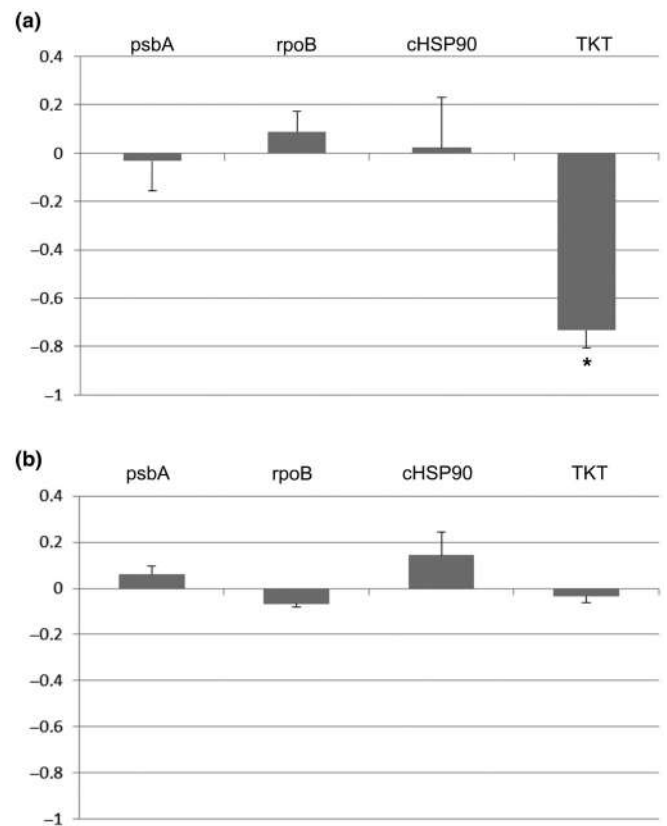


Fig. 5 Accumulation levels of *psbA*, *rpoB*, *cHSP90* and transketolase (TKT) mRNAs in symptomatic (a) and non-symptomatic (b) tissues with respect to mock-inoculated chrysanthemum plants determined by RT-qPCR. The reported data are the mean of at least three independent experiments. The elongation factor 1 α (EF1 α) was used as the internal reference gene for normalization. Results are presented as log₁₀ fold-change. Bars indicate SE. Duncan's multiple range test: *, $P \leq 0.05$.

in the mRNA accumulation were detected between green and chlorotic tissue (Fig. 5). More specifically, the relative levels of two plastid-encoded transcripts (the mRNAs of the *rpoB* subunit of the bacterial-like RNA polymerase and of the *psbA* component of photosystem II) and of one nuclear-encoded transcript (the mRNA of *cHSP90*, the chloroplastic heat-shock protein 90), remained essentially the same. By contrast, a pronounced reduction in the TKT transcript was specifically observed in the chlorotic tissue (Fig. 5).

Finally, to further discard that the remaining mRNA encoding the chloroplastic TKT might still serve to produce the corresponding protein at the physiological level, we took advantage of the existence of a commercially available antibody against this enzyme. Western blot analyses revealed that its accumulation was significantly lower in the chlorotic sectors than in their green counterparts of the same CChMVd-infected leaves and of leaves from mock-inoculated plants (Fig. 6). Altogether, these results firmly uphold the notion that CChMVd initiates disease via a viroid-sRNA containing the pathogenic determinant, which guides RISC(AGO1) to cleave the mRNA encoding the chloroplastic TKT, thus downregulating its accumulation.

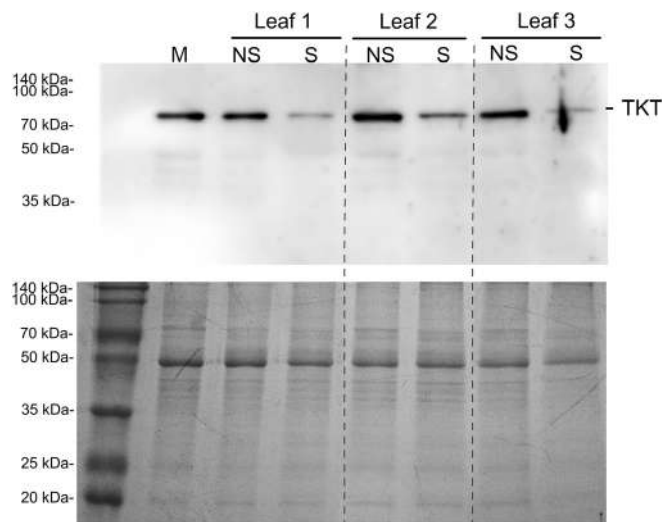


Fig. 6 Western blot analysis detection of transketolase (TKT) in protein extracts from symptomatic (S) and non-symptomatic (NS) sectors of leaves infected with CChMVd-S (CM20) variant and from a mock-inoculated (M) chrysanthemum plant. Equal loading was assessed by Coomassie blue staining (lower panel). Broken vertical lines indicate irrelevant lanes removed from the gel and membrane.

A gain-of-function mutant of CChMVd supports the proposed mechanism of disease initiation

Our previous data, showing that even a single substitution in the UUUC tetraloop results in loss-of-function mutants (conversion of a pathogenic variant into a latent one; Figs 1, S2), support that the formation of the hybrid between the CChMVd-sRNA3 and the TKT mRNA is crucial for initiating disease. In such mutants, the stability of the hybrid is compromised in the positions proximal to the 5' terminus of the CChMVd-sRNA3, which are known to be critical for proper hybrid formation between miRNAs and their targets (Fahlgren & Carrington, 2010).

To further strengthen the involvement of RNA silencing in initiating disease, we focussed on constructing a gain-of-function mutant. Since in the hybrid between the mRNA encoding the chloroplastic TKT and the CChMVd-sRNA3, there is a mismatch at position 7 (counting from the 5'-terminus of the latter; Fig. 7b), we reasoned that replacing the C at this position by a U would result in a U–A Watson–Crick base-pair that should increase the stability of the hybrid and favour a more efficient cleavage. If so, earlier or more severe symptoms should be expected. Importantly, this position 7 in the CChMVd-sRNA corresponds to position C89 in the genomic viroid RNA (variant CM20), with such substitution resulting in the conversion of a C–G base-pair into a U–G wobble pair (Fig. 7a) that should not distort the proposed secondary structure of the viroid and its infectivity.

Inoculation of chrysanthemum blocks (containing 10 plants each) with equal amounts of *in vitro* dimeric head-to-tail transcripts from the wild-type symptomatic variant (CM20) or its C89→U variant (CM20-U89mut), showed that: the latter was as infectious as the former, since all plants of each block eventually expressed symptoms; and the C89→U variant incited earlier and

more severe symptoms than its wild-type counterpart (Fig. 7c,d). Therefore, the phenotype incited by the mutant variant agreed with the proposed mechanism of pathogenesis. To add further credence to this view, we analysed the resulting progeny (Fig. S6). In early symptomatic leaves (14 dpi), four of six variants from the chlorotic sectors preserved the C89→U substitution, while this position reverted to the wild-type C89 in five of six variants from the green sectors. In intermediate symptomatic leaves (21 dpi), two of six variants from the chlorotic sectors preserved the C89→U substitution, while in six of six variants from the green sectors, this position reverted to the wild-type C89. Finally, in late symptomatic leaves (28 dpi), the mutated position reverted to the wild-type C89 in all variants from the chlorotic and green sectors. These results clearly indicate that, although viable, variants with the C89→U change have a lower fitness (consistent with their lower progeny accumulation, see above) than those with the wild-type C89, with the latter eventually coming to dominate the progeny. Regarding the pathogenic determinant (the tetraloop UUUC, positions 82–85), it was preserved in all variants from chlorotic sectors, while point mutations were detected in the corresponding tetraloop in 4/6, 6/6 and 4/6 variants from the green sectors of symptomatic leaves at early, intermediate and late stages, respectively, in agreement with previous observations (Fig. 2).

Discussion

Viroids accumulate in an infected host as populations of slightly different sequence variants, thus showing the typical features of quasispecies (Codoñer *et al.*, 2006; Brass *et al.*, 2017). Sequence variability in a viroid population is mainly generated by the error-prone polymerases involved in replication and, on such a variability, natural selection acts to generate the observed infecting viroid populations. How combination of variability and selection pressure may affect host colonization and viroid pathogenesis is largely unknown. In this study, we analysed the progeny viroid variants in the leaves of chrysanthemum, the CChMVd natural host, inoculated with a single symptomatic variant of this viroid, which contains the pathogenic determinant previously mapped at a UUUC tetraloop (de la Peña *et al.*, 1999). At 20 dpi, the progeny was already composed of variants containing the original pathogenic determinant (CChMVd-S) and variants in which such a motif was mutated (CChMVd-NS). These different variants showed a clear spatial segregation even in a single symptomatic leaf: CChMVd-S variants were prevalent in the chlorotic sectors of symptomatic leaves, while the CChMVd-NS variants were prevalently present in nonsymptomatic tissues. Therefore, a strict association between variants containing the pathogenic determinant and the symptoms was observed. Importantly, both type of variants accumulated at similar levels in the symptomatic and nonsymptomatic sectors, excluding a possible direct role of the pathogenic determinant on the viroid variants accumulation in the infected tissues. These findings showed that, although the inoculated CChMVd (S) variants persisted in the plant and preserved their ability of eliciting the specific symptom, the progeny in the

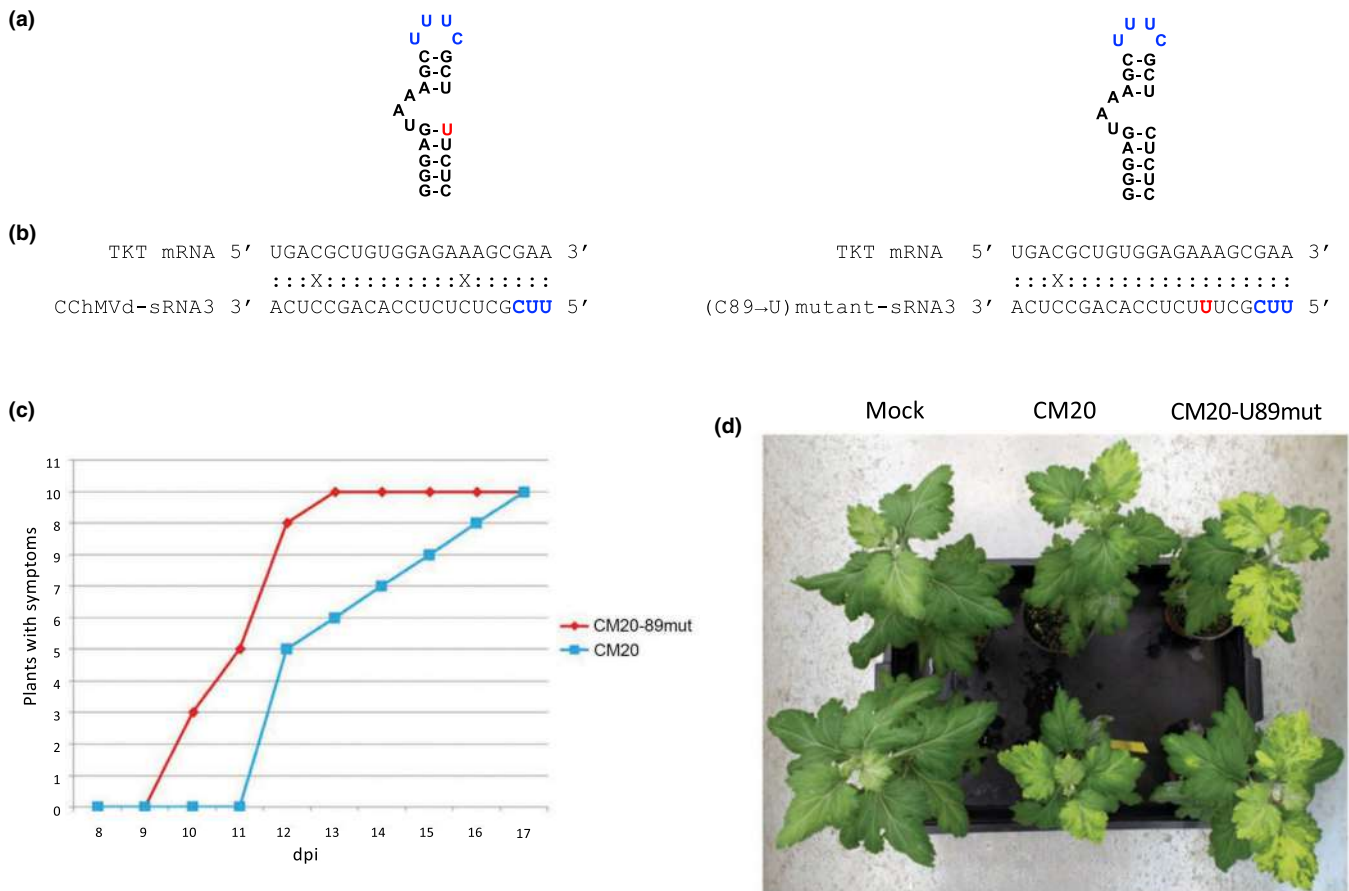


Fig. 7 Earlier and more severe symptoms induced by a gain-of-function CChMVd mutant variant in chrysanthemum. Schematic representation of the pathogenic region containing the tetraloop UUUC (in blue) of the variant CM20 (left) and of the mutant variant CM20-U89mut (right), in which the C at position 89 has been replaced by a U (in red) (a). Hybrid between the mRNA encoding the chloroplastic TKT and the CChMVd-sRNA3 from the CM20 (left) and CM20-U89mut (right) variants (b). Time course (days postinoculation, dpi) of symptom expression in chrysanthemum plants inoculated with the CM20 and CM20-U89mut variants (c). Representative mock-inoculated and symptomatic chrysanthemum plants infected by the CM20 and CM20-U89mut variants (d).

nonsymptomatic leaf tissues evolved mainly in variants lacking the pathogenic determinant. The nonsymptomatic infections resulting from inoculation of CChMVd-NS variants (replacing the tetraloop UUUC with another one) and the absence of the UUUC pathogenic determinant in the progeny from the infected plants further confirmed this conclusion. Moreover, the identification of CChMVd-S variants (with a tetraloop UUUC) in the progeny from a very small chlorotic area that appeared at a late infection stage (28 dpi) in a plant inoculated with a CChMVd-NS, showed that the evolution of S from NS variants is also possible, although it is quite rare. Bioassays and early characterization of viroid progeny populations highlighted that the S variants move systemically within the host in the first 5 dpi and that a longer period of time (between 5 and 20 dpi) is needed for the new symptomless CChMVd-NS variants to be generated and become prevalent in green tissues of plants inoculated with CChMVd-S variants. Altogether, these findings showed CChMVd segregating populations even in a single leaf. The fact that only one tetraloop at the pathogenic domain is able to trigger symptoms, while most variants lacking such a motif are nonsymptomatic, generates a population bottleneck in the infected

hosts that correlates with the symptom expression and may represent the different evolutionary trajectories observed in S and NS CChMVd variants.

In the absence of an annotated chrysanthemum genome, the *de novo* assembly of the transcriptome of ‘Bonnie Jean’ chrysanthemum leaves was performed in this study. This effort provided a data set of mRNAs actually expressed in our experimental host that, by adopting very stringent constraints, allowed the identification of the TKT mRNA as the target of CChMVd-sRNA3 for its RNA silencing-mediated degradation. This finding is supported by several solid evidence: RLM-RACE experiments showed that TKT mRNA is cleaved at the expected site according to an AGO-mediated cleavage driven by CChMVd-sRNA3 in chlorotic tissues, but not in green tissues; a single-nucleotide change at a position that increases the stability of the hybrid between the CChMVd-sRNA3 and the TKT mRNA, while not affecting viroid infectivity, does enhance symptom severity; and RT-qPCR and Western blot revealed that the TKT mRNA and protein, respectively, accumulate at lower levels in the chlorotic tissues, a finding fully consistent with the chlorosis incited by the reduction in transketolase activity in tobacco and *N. benthamiana*

reported previously (Henkes *et al.*, 2001; Yuan *et al.*, 2011). The direct correlation between the lower steady state level of mRNA and the encoded protein should not be taken for granted because transcript profiling neither accounts for post-transcriptional modifications nor for non-translated transcripts during some developmental stages, thus highlighting the importance of assessing protein levels (Shrestha *et al.*, 2020).

It is worth noting that lower accumulation of TKT mRNA and protein were restricted to the chlorotic tissues of the mottled leaves infected by CChMVd. In these tissues, both the variants containing the pathogenic determinant and the CChMVd-sRNA3 were prevalent with respect to the green sectors, thus providing a consistent picture linking the segregation pattern of CChMVd-S and -NS variants with the molecular lesion incited through RNA silencing by the CChMVd-sRNA3 and the observed chlorotic macroscopic symptom. In short, these results support that RNA silencing has a major role in triggering the initial lesion caused by CChMVd.

We have recently established a distinction between viroid-induced symptoms: whereas those typically incited by PSTVd and related members of the *Pospiviroidae* are non-specific and systemic, those elicited by most members of the *Avsunviroidae* are specific and local, for example closely associated with variants containing a specific pathogenic determinant (Flores *et al.*, 2020; Navarro *et al.*, 2021a). We have shown that PLMVd variants causing PC and PYM initiate disease (distinct chloroses) by vd-sRNA-induced RNA silencing of mRNAs that encode proteins (a heat-shock protein and a thylakoid translocase subunit, respectively) mediating chloroplast biogenesis/development (Navarro *et al.*, 2012; Delgado *et al.*, 2019). Here, we have extended this view to CChMVd, which we propose triggers its characteristic mottle by silencing the mRNA coding for the chloroplastic TKT. CChMVd-sRNAs are mostly of 21 nt, as those generated by other pelamoviroids, such as PLMVd (Di Serio *et al.*, 2009; Bolduc *et al.*, 2010; Navarro *et al.*, 2012; Delgado *et al.*, 2019) and apple hammerhead viroid (Zhang *et al.*, 2014; Serra *et al.*, 2018). By contrast, the most abundant vd-sRNAs produced by typical members of the family *Pospiviroidae* are of 21- and 22-nt accompanied by significant levels of the 24-nt species (Machida *et al.*, 2007; Navarro *et al.*, 2009; Di Serio *et al.*, 2010; Martínez *et al.*, 2010; Wang *et al.*, 2011; Zhang *et al.*, 2014; Adkar-Purushothama *et al.*, 2015). Thus, the defensive RNA silencing machinery operates differently in the two families (Flores *et al.*, 2020). The analyses of CChMVd-sRNAs further showed that those containing the pathogenic determinant accumulated prevalently in the chlorotic sectors, paralleling the biased accumulation in these tissues of CChMVd-S.

For PSTVd and related viroids (inducing non-specific phenotypes like stunting but also some chloroses), the situation appears different (Flores *et al.*, 2020). Particularly, the chlorosis induced by the nuclear replicating viroid CSVd (family *Pospiviroidae*) in chrysanthemum (Fig. 2) is not associated with specific viroid variants. This is in sharp contrast with the situation observed for CChMVd (family *Avsunviroidae*) in the same host, thus excluding a specific correlation between evolutionary routes of the inocula and the appearance of chlorotic areas in the symptomatic

leaves. This also points out a clear distinction between members of the two viroid families.

Remarkably, the symptom incited by the yellow satellite RNA (Y-sat) of cucumber mosaic virus (CMV) in tobacco (a bright yellowing) (Takanami, 1981), resembles the above-mentioned characteristics of some members of the *Avsunviroidae*. Furthermore, a common mechanism has been posited: Y-sat sRNA, PC- and PYM-sRNAs, and now CChMVd-sRNA of 22- or 21-nt with the corresponding pathogenic determinants have 5'-terminal Us, involving RISC(AGO1)-mediated cleavage of their cognate mRNAs in what likely are the primary lesions eventually eliciting disease symptoms (Shimura *et al.*, 2011; Smith *et al.*, 2011; Navarro *et al.*, 2012; Delgado *et al.*, 2019; this work). The observation that all these sRNAs have more than one 5'-terminal U (while AGO1 needs only one for loading) is intriguing. By becoming thermodynamically unstable, the corresponding end of the vd-sRNA/mRNA duplexes could provide some advantage (e.g. recruiting regulatory factors that remodel the duplex or affect AGO strand loading preference in a context-dependent mode; Medley *et al.*, 2021).

However, when it comes to the host colonization, there is an important difference between the Y-sat on the one side, and PLMVd and CChMVd on the other. The first one appears genetically stable, with the difference between yellow and green tissues probably reflecting whether or not they have been invaded by the satellite RNA. By contrast, symptomatic and nonsymptomatic tissues (including sectors of the same leaf) are infected by pathogenic and latent variants of the two viroids, respectively (Navarro *et al.*, 2012; Delgado *et al.*, 2019; this work). This uneven distribution of variants most likely results from: the extremely high mutation rate of CChMVd and possibly of PLMVd; the strong competition between variants leading to superinfection exclusion; and the existence of bottlenecks during host colonization. In support of the first point, there is direct and indirect evidence for CChMVd (Gago *et al.*, 2009) and PLMVd (Ambrós *et al.*, 1999; Glouzon *et al.*, 2014) or AHVd (Serra *et al.*, 2018; Chiumenti *et al.*, 2019), respectively. Regarding the second point, co-infections or consecutive (separated by a time interval) experimental infections with two variants of either CChMVd or PLMVd has revealed distinct peaks in the fitness landscape (de la Peña & Flores, 2002; Serra *et al.*, 2017). On the third point, symptomatic variants of CChMVd can evolve into nonsymptomatic ones accumulating in green leaf sectors (this work), despite the higher fitness of the former with respect to the latter (de la Peña & Flores, 2002). This result strongly suggests that, as previously discussed for plant viruses (Gutiérrez *et al.*, 2012; Zwart & Elena, 2015), a small number of viroid molecules infect different leaf sectors and may exclude colonization by other variants, thus unveiling the role of random effects of genetic drift in viroid evolution during host colonization. In plant viruses, the mechanistic framework involved in bottleneck and superinfection dynamics is far from being completely understood, although there is evidence that it is a complex phenomenon relying on both specific virus-encoded proteins/ORFs and RNA silencing (Donaire *et al.*, 2016; Qu *et al.*, 2020). In the case of positive-sense RNA viruses, which possess a genome from which viral

proteins are directly translatable, a major role has been attributed to virus-encoded bottleneck-enforcing proteins (BNEPs; reviewed by Perdoncini Carvalho *et al.*, 2022). Bottleneck-enforcing proteins are viral proteins that, when accumulate at high intracellular concentration, are able to repress the replication of their own encoding genomes, thus determining strong population bottlenecks that allow only few bottleneck-escaping genome copies to succeed in embarking replication and become prevalent in the cell (Perdoncini Carvalho *et al.*, 2022). Interestingly, sometimes BNEP are proteins involved also in virus replication, thus exerting two opposite functions (Zhang *et al.*, 2017; Perdoncini Carvalho *et al.*, 2022). In the case of viroids, which do not encode proteins but are still targeted by RNA silencing machinery, the bottleneck and superinfection exclusion dynamics take place in the absence of pathogen-derived proteins, thus suggesting a major contribution of RNA-based mechanisms and/or host-derived proteins to this phenomenon. Therefore, viroids may provide useful experimental systems to further assess the mechanisms involved in the sequence variability of infectious RNAs during host colonization.

In summary, we present data supporting that the chlorotic mottle incited by CChMVd variants with a specific tetranucleotide (UUUC) is initiated by a CChMVd-sRNA harbouring most of this pathogenic determinant. Moreover, the distribution pattern of such chlorosis reflects the spatial and evolutionary behaviour of the pathogenic variants in the infected host, thus being clearly distinguished from the chloroses incited by nuclear-replicating viroids such as CSVd (this work) and by many viruses (Zhao *et al.*, 2016; Seo *et al.*, 2018). In these cases, chloroses are possibly elicited by signalling routes between chloroplasts (with a major role in defence) and nuclei (Seay *et al.*, 2009; Chi *et al.*, 2013; Chan *et al.*, 2016). This different ‘colonization behavior’ likely depends, among other factors, on the significantly diverse viroid mutation rate shown by members of the two viroid families (López-Carrasco *et al.*, 2017; but see Wu & Bisaro, 2020).

Acknowledgements

We thank Miryam Perez Cañas and Carmen Hernández for their help in Western blot experiments. We also want to thank the editor and reviewers of this paper for helpful suggestions. This project has been funded by Ministerio de Economía y Competitividad of Spain, Grant BFU 2014-56812-P. Open Access Funding provided by Consiglio Nazionale delle Ricerche within the CRUI-CARE Agreement.





Competing interests

None declared.

Author contributions

RF, PS, BN and FDS designed the research. PS, BN and SG-Z performed the research. AG and JF analysed the bioinformatics data. RF and FDS wrote the paper.

ORCID

Francesco Di Serio  <https://orcid.org/0000-0003-2822-704X>
Ricardo Flores  <https://orcid.org/0000-0002-3033-5077>
Javier Forment  <https://orcid.org/0000-0002-1872-4061>
Selma Gago-Zachert  <https://orcid.org/0000-0002-1084-2119>
Andreas Gisel  <https://orcid.org/0000-0001-7218-9488>
Beatriz Navarro  <https://orcid.org/0000-0001-8981-1018>
Pedro Serra  <https://orcid.org/0000-0003-4229-6906>

Data availability

High-throughput sequencing data of this study were deposited in NCBI Sequence Read Archive (SRA) under BioProject ID: PRJNA906930. GenBank accession nos. of CChMVd variants are from OP918681 to OP918845.

References

- Adkar-Purushothama CR, Brosseau C, Giguère T, Sano T, Moffett P, Perreault JP. 2015. Small RNA derived from the virulence modulating region of the potato spindle tuber viroid silences callose synthase genes of tomato plants. *Plant Cell* 27: 2178–2194.
- Adkar-Purushothama CR, Perreault JP. 2020. Current overview on viroid-host interactions. *Wiley Interdisciplinary Reviews RNA* 11: e1570.
- Ambrós S, Hernández C, Flores R. 1999. Rapid generation of genetic heterogeneity in progenies from individual cDNA clones of peach latent mosaic viroid in its natural host. *Journal of General Virology* 80: 2239–2252.
- Bewick V, Cheek L, Ball J. 2004. Statistics review 9: one-way analysis of variance. *Critical Care* 8: 130–136.
- Bolduc F, Hoareau C, St-Pierre P, Perreault JP. 2010. In-depth sequencing of the siRNAs associated with peach latent mosaic viroid infection. *BMC Molecular Biology* 11: 16.
- Brass JR, Owens RA, Matoušek J, Steger G. 2017. Viroid quasispecies revealed by deep sequencing. *RNA Biology* 14: 317–325.
- Bussière F, Ouellet J, Côté F, Lévesque D, Perreault JP. 2000. Mapping in solution shows the peach latent mosaic viroid to possess a new pseudoknot in a complex, branched secondary structure. *Journal of Virology* 74: 2647–2654.
- Chan KX, Phua SY, Crisp P, McQuinn R, Pogson BJ. 2016. Learning the languages of the chloroplast: retrograde signaling and beyond. *Annual Review of Plant Biology* 67: 25–53.
- Chi W, Sun X, Zhang L. 2013. Intracellular signaling from plastid to nucleus. *Annual Review of Plant Biology* 64: 559–582.
- Chiumenti M, Navarro B, Venerito P, Civita F, Minafra A, Di Serio F. 2019. Molecular variability of apple hammerhead viroid from Italian apple varieties supports the relevance *in vivo* of its branched conformation stabilized by a kissing loop interaction. *Virus Research* 270: 197644.
- Codoñer FM, Darós JA, Solé RV, Elena SF. 2006. The fittest versus the flattest: experimental confirmation of the quasispecies effect with subviral pathogens. *PLoS Pathogens* 2: e136.
- Dai X, Zhuang Z, Zhao PX. 2018. psRNATarget: a plant small RNA target analysis server (2017 release). *Nucleic Acids Research* 46: W49–W54.
- Delgado S, Navarro B, Serra P, Gentit P, Cambra MÁ, Chiumenti M, De Stradis A, Di Serio F, Flores R. 2019. How sequence variants of a plastid-replicating viroid with one single nucleotide change initiate disease in its natural host. *RNA Biology* 16: 906–917.
- Di Serio F, Gisel A, Navarro B, Delgado S, Martínez de Alba AE, Donvito G, Flores R. 2009. Deep sequencing of the small RNAs derived from two symptomatic variants of a chloroplastic viroid: implications for their genesis and for pathogenesis. *PLoS ONE* 4: e7539.

- Di Serio F, Li SF, Matoušek J, Owens RA, Pallás V, Randles JW, Sano T, JTJ V, Vidalakis G, Flores R *et al.* 2018. ICTV virus taxonomy profile: *Avsunviroidae*. *Journal of General Virology* 99: 611–612.
- Di Serio F, Li SF, Matoušek J, Owens RA, Pallás V, Randles JW, Sano T, JTJ V, Vidalakis G, Flores R *et al.* 2021. ICTV virus taxonomy profile: *Pospiviroidae*. *Journal of General Virology* 102: 001543.
- Di Serio F, Martínez de Alba AE, Navarro B, Gisel A, Flores R. 2010. RNA-dependent RNA polymerase 6 delays accumulation and precludes meristem invasion of a viroid that replicates in the nucleus. *Journal of Virology* 84: 2477–2489.
- Diener TO. 1971. Potato spindle tuber “virus”: IV. A replicating, low molecular weight RNA. *Virology* 45: 411–428.
- Diener TO. 2003. Discovering viroids – a personal perspective. *Nature Reviews Microbiology* 1: 75–80.
- Ding B. 2009. The biology of viroid-host interactions. *Annual Review of Phytopathology* 47: 105–131.
- Donaire L, Burguán J, García-Arenal F. 2016. RNA silencing may play a role in but is not the only determinant of the multiplicity of infection. *Journal of Virology* 90: 553–561.
- Emanuelsson O, Nielsen H, von Heijne G. 1999. ChloroP, a neural network-based method for predicting chloroplast transit peptides and their cleavage sites. *Protein Science* 8: 978–984.
- Fahlgren N, Carrington JC. 2010. miRNA target prediction in plants. *Methods in Molecular Biology* 592: 51–57.
- Fang X, Qi Y. 2016. RNAi in plants: an Argonaute-centered view. *Plant Cell* 28: 272–285.
- Flores R, Navarro B, Delgado S, Serra P, Di Serio F. 2020. Viroid pathogenesis: a critical appraisal of the role of RNA silencing in triggering the initial molecular lesion. *FEMS Microbiology Reviews* 44: 386–398.
- Gago S, de la Peña M, Flores R. 2005. A kissing-loop interaction in a hammerhead viroid RNA critical for its *in vitro* folding and *in vivo* viability. *RNA* 11: 1073–1083.
- Gago S, Elena SF, Flores R, Sanjuán R. 2009. Extremely high mutation rate of a hammerhead viroid. *Science* 323: 1308.
- Giguère T, Adkar-Purushothama C, Perreault JP. 2014. Comprehensive secondary structure elucidation of four genera of the family Pospiviroidae. *PLoS ONE* 9: e98655.
- Glouzon JP, Bolduc F, Wang S, Najmanovich RJ, Perreault JP. 2014. Deep-sequencing of the peach latent mosaic viroid reveals new aspects of population heterogeneity. *PLoS ONE* 9: e87297. [Published correction appears in *PLoS ONE*, 9: e96229].
- Gross HJ, Domdey H, Lossow C, Jank P, Raba M, Alberty H, Sängler HL. 1978. Nucleotide sequence and secondary structure of potato spindle tuber viroid. *Nature* 273: 203–208.
- Gutiérrez S, Michalakakis Y, Blanc S. 2012. Virus population bottlenecks during within-host progression and host-to-host transmission. *Current Opinion in Virology* 2: 546–555.
- Henkes S, Sonnewald U, Badur R, Flachmann R, Stitt M. 2001. A small decrease of plastid transketolase activity in antisense tobacco transformants has dramatic effects on photosynthesis and phenylpropanoid metabolism. *Plant Cell* 13: 535–551.
- Hernández C, Flores R. 1992. Plus and minus RNAs of peach latent mosaic viroid self-cleave *in vitro* via hammerhead structures. *Proceedings of the National Academy of Sciences, USA* 89: 3711–3715.
- Hutchins CJ, Rathjen PD, Forster AC, Symons RH. 1986. Self-cleavage of plus and minus RNA transcripts of avocado sunblotch viroid. *Nucleic Acids Research* 14: 3627–3640.
- Kovalskaya N, Hammond RW. 2014. Molecular biology of viroid-host interactions and disease control strategies. *Plant Science* 228: 48–60.
- Lawson RH. 1987. Chrysanthemum stunt viroid. In: Diener TO, ed. *The viroids*. New York, NY, USA: Plenum Press, 247–259.
- Livak KJ, Schmittgen TD. 2001. Analysis of relative gene expression data using real-time quantitative PCR and the $2^{-\Delta\Delta Ct}$ method. *Methods* 25: 402–408.
- López-Carrasco A, Ballesteros C, Sentandreu V, Delgado S, Gago-Zachert S, Flores R, Sanjuán R. 2017. Different rates of spontaneous mutation of chloroplastic and nuclear viroids as determined by high-fidelity ultra-deep sequencing. *PLoS Pathogens* 13: e1006547.
- Ma Z, Zhang X. 2018. Actions of plant Argonautes: predictable or unpredictable? *Current Opinion in Plant Biology* 45: 59–67.
- Machida S, Yamahata N, Watanuki H, Owens RA, Sano T. 2007. Successive accumulation of two size classes of viroid-specific small RNA in potato spindle tuber viroid-infected tomato plants. *Journal of General Virology* 88: 3452–3457.
- Mallory A, Vaucheret H. 2010. Form, function, and regulation of ARGONAUTE proteins. *Plant Cell* 22: 3879–3889.
- Martínez de Alba AE, Flores R, Hernández C. 2002. Two chloroplastic viroids induce the accumulation of the small RNAs associated with post-transcriptional gene silencing. *Journal of Virology* 76: 13094–13096.
- Martínez G, Donaire L, Llave C, Pallas V, Gomez G. 2010. High-throughput sequencing of Hop stunt viroid-derived small RNAs from cucumber leaves and phloem. *Molecular Plant Pathology* 11: 347–359.
- McInnes JL, Symons RH. 1991. Comparative structure of viroids and their rapid detection using radioactive and nonradioactive nucleic acid probes. In: Maramorosch K, ed. *Viroids and satellites: molecular parasites at the frontier of life*. Boca Raton, FL, USA: CRC Press, 21–58.
- Medley JC, Panzade G, Zinovyeva AY. 2021. MicroRNA strand selection: unwinding the rules. *Wiley Interdisciplinary Reviews RNA* 12: e1627.
- Mi S, Cai T, Hu Y, Chen Y, Hodges E, Ni F, Wu L, Li S, Zhou H, Long C *et al.* 2008. Sorting of small RNAs into Arabidopsis argonaute complexes is directed by the 5' terminal nucleotide. *Cell* 133: 116–127.
- Minoia S, Carbonell A, Di Serio F, Gisel A, Carrington JC, Navarro B, Flores R. 2014. Specific ARGONAUTES bind selectively small RNAs derived from potato spindle tuber viroid and attenuate viroid accumulation *in vivo*. *Journal of Virology* 88: 11933–11945.
- Montgomery TA, Howell MD, Cuperus JT, Li D, Hansen JE, Alexander AL, Chapman EJ, Fahlgren N, Allen E, Carrington JC. 2008. Specificity of ARGONAUTE7-miR390 interaction and dual functionality in TAS3 trans-acting siRNA formation. *Cell* 133: 128–141.
- Navarro B, Flores R. 1997. Chrysanthemum chlorotic mottle viroid: unusual structural properties of a subgroup of self-cleaving viroids with hammerhead ribozymes. *Proceedings of the National Academy of Sciences, USA* 94: 11262–11267.
- Navarro B, Flores R, Di Serio F. 2021a. Advances in viroid-host interactions. *Annual Review of Virology* 8: 305–325.
- Navarro B, Gisel A, Rodio ME, Delgado S, Flores R, Di Serio F. 2012. Small RNAs containing the pathogenic determinant of a chloroplast-replicating viroid guide the degradation of a host mRNA as predicted by RNA silencing. *The Plant Journal* 70: 991–1003.
- Navarro B, Gisel A, Serra P, Chiumenti M, Di Serio F, Flores R. 2021b. Degradome analysis of tomato and *Nicotiana benthamiana* plants infected with potato spindle tuber viroid. *International Journal of Molecular Sciences* 22: 3725.
- Navarro B, Pantaleo V, Gisel A, Moxon S, Dalmay T, Bisztray G, Di Serio F, Burguán J. 2009. Deep sequencing of viroid-derived small RNAs from grapevine provides new insights on the role of RNA silencing in plant-viroid interaction. *PLoS ONE* 4: e7686.
- Papaefthimiou I, Hamilton A, Denti M, Baulcombe D, Tsagris M, Tabler M. 2001. Replicating potato spindle tuber viroid RNA is accompanied by short RNA fragments that are characteristic of post-transcriptional gene silencing. *Nucleic Acids Research* 29: 2395–2400.
- de la Peña M, Flores R. 2002. Chrysanthemum chlorotic mottle viroid RNA: dissection of the pathogenicity determinant and comparative fitness of symptomatic and non-symptomatic variants. *Journal of Molecular Biology* 321: 411–421.
- de la Peña M, Navarro B, Flores R. 1999. Mapping the molecular determinant of pathogenicity in a hammerhead viroid: a tetraloop within the *in vivo* branched RNA conformation. *Proceedings of the National Academy of Sciences, USA* 96: 9960–9965.
- Perdoncini Carvalho C, Ren R, Han J, Qu F. 2022. Natural selection, intracellular bottlenecks of virus populations, and viral superinfection exclusion. *Annual Review of Virology* 9: 121–137.
- Poulsen C, Vaucheret H, Brodersen P. 2013. Lessons on RNA silencing mechanisms in plants from eukaryotic argonaute structures. *Plant Cell* 25: 22–37.
- Qu F, Zheng L, Zhang S, Sun R, Slot J, Miyashita S. 2020. Bottleneck, Isolate, Amplify, Select (BIAS) as a mechanistic framework for intracellular population dynamics of positive-sense RNA viruses. *Virus Evolution* 6: veaa086.

- Rehmsmeier M, Steffen P, Hochsmann M, Giegerich R. 2004. Fast and effective prediction of microRNA/target duplexes. *RNA* 10: 1507–1517.
- Rogers K, Chen X. 2013. Biogenesis, turnover, and mode of action of plant microRNAs. *Plant Cell* 25: 2383–2399.
- Schulz MH, Zerbino DR, Vingron M, Birney E. 2012. Oases: robust *de novo* RNA-Seq assembly across the dynamic range of expression levels. *Bioinformatics* 28: 1086–1092.
- Seay M, Hayward AP, Tsao J, Dinesh-Kumar SP. 2009. Something old, something new: plant innate immunity and autophagy. *Current Topics in Microbiology and Immunology* 335: 287–306.
- Seo JK, Kim MK, Kwak HR, Choi HS, Nam M, Choe J, Choi B, Han SJ, Kang JH, Jung C. 2018. Molecular dissection of distinct symptoms induced by tomato chlorosis virus and tomato yellow leaf curl virus based on comparative transcriptome analysis. *Virology* 516: 1–20.
- Serra P, Bertolini E, Martínez MC, Cambra M, Flores R. 2017. Interference between variants of peach latent mosaic viroid reveals novel features of its fitness landscape: implications for detection. *Scientific Reports* 7: 42825.
- Serra P, Messmer A, Sanderson D, James D, Flores R. 2018. Apple hammerhead viroid-like RNA is a bona fide viroid: autonomous replication and structural features support its inclusion as a new member in the genus *Pelamoviroid*. *Virus Research* 249: 8–15.
- Shimura H, Pantaleo V, Ishihara T, Myojo N, Inaba J, Sueda K, Burgyán J, Masuta C. 2011. A viral satellite RNA induces yellow symptoms on tobacco by targeting a gene involved in chlorophyll biosynthesis using the RNA silencing machinery. *PLoS Pathogens* 7: e1002021.
- Shrestha A, Mishra AK, Matoušek J, Steinbachová L, Potěšil D, Nath VS, Awasthi P, Kocábek T, Jakse J, Drábková LZ *et al.* 2020. Integrated proteo-transcriptomic analyses reveal insights into regulation of pollen development stages and dynamics of cellular response to apple fruit crinkle viroid (AFCVd)-infection in *Nicotiana tabacum*. *International Journal of Molecular Sciences* 21: 8700.
- Sievers F, Higgins DG. 2014. CLUSTAL OMEGA, accurate alignment of very large numbers of sequences. *Methods in Molecular Biology* 1079: 105–116.
- Smith NA, Eamens AL, Wang M-B. 2011. Viral small interfering RNAs target host genes to mediate disease symptoms in plants. *PLoS Pathogens* 7: e1002022.
- Steger G, Riesner D. 2018. Viroid research and its significance for RNA technology and basic biochemistry. *Nucleic Acids Research* 46: 10563–10576.
- Symons RH. 1981. Avocado sunblotch viroid: primary sequence and proposed secondary structure. *Nucleic Acids Research* 9: 6527–6537.
- Takanami Y. 1981. A striking change in symptoms on cucumber mosaic virus-infected tobacco plants induced by satellite RNA. *Virology* 109: 120–126.
- Wang MB, Bian XY, Wu LM, Liu LX, Smith NA, Isenegger D, Wu RM, Masuta C, Vance VB, Watson JM *et al.* 2004. On the role of RNA silencing in the pathogenicity and evolution of viroids and viral satellites. *Proceedings of the National Academy of Sciences, USA* 101: 3275–3280.
- Wang Y, Shibuya M, Taneda A, Kurauchi T, Senda M, Owens RA, Sano T. 2011. Accumulation of Potato spindle tuber viroid-specific small RNAs is accompanied by specific changes in gene expression in two tomato cultivars. *Virology* 413: 72–83.
- Wang Y, Zirbel CL, Leontis NB, Ding B. 2018. RNA 3-dimensional structural motifs as a critical constraint of viroid RNA evolution. *PLoS Pathogens* 14: e1006801.
- Wu J, Bisaro DM. 2020. Biased Pol II fidelity contributes to conservation of functional domains in the potato spindle tuber viroid genome. *PLoS Pathogens* 16: e1009144.
- Wu J, Zhou C, Li J, Li C, Tao X, Leontis NB, Zirbel CL, Bisaro DM, Ding B. 2020. Functional analysis reveals G/U pairs critical for replication and trafficking of an infectious non-coding viroid RNA. *Nucleic Acids Research* 48: 3134–3155.
- Yuan C, Li C, Yan L, Jackson AO, Liu Z, Han C, Yu J, Li D. 2011. A high throughput barley stripe mosaic virus vector for virus induced gene silencing in monocots and dicots. *PLoS ONE* 6: ve26468.
- Zerbino DR, Birney E. 2008. Velvet: algorithms for *de novo* short read assembly using de Bruijn graphs. *Genome Research* 18: 821–829.
- Zhang XF, Sun R, Guo Q, Zhan S, Meulia T, Halfmann R, Li D, Qu F. 2017. A self-perpetuating repressive state of a viral replication protein blocks superinfection by the same virus. *PLoS Pathogens* 13: e1006253.
- Zhang Z, Qi S, Tang N, Zhang X, Chen S, Zhu P, Ma L, Cheng J, Xu Y, Lu M *et al.* 2014. Discovery of replicating circular RNAs by RNA-Seq and computational algorithms. *PLoS Pathogens* 10: e1004553.
- Zhao JH, Hua CL, Fang YY, Guo HS. 2016. The dual edge of RNA silencing suppressors in the virus-host interactions. *Current Opinion in Virology* 17: 39–44.
- Zwart MP, Elena SF. 2015. Matters of size: genetic bottlenecks in virus infection and their potential impact on evolution. *Annual Review of Virology* 2: 161–179.

Supporting Information

Additional Supporting Information may be found online in the Supporting Information section at the end of the article.

Dataset S1 Sequences of the chrysanthemum transcripts identified by transcriptome analysis and used to generate specific primers for RT-qPCR and RLM-RACE assays.

Fig. S1 Detection of chrysanthemum chlorotic mottle viroid and chrysanthemum stunt viroid by Northern blot hybridization assays.

Fig. S2 Analysis of symptom expression and viroid progeny accumulating in chrysanthemum plants inoculated with chrysanthemum chlorotic mottle viroid variants containing AUUU, AAUU or UUUU tetraloop.

Fig. S3 Progeny variants of chrysanthemum chlorotic mottle viroid pathogenic variant (CM20) at 5 dpi from upper noninoculated leaves.

Fig. S4 Alignment of CSVd progeny variants.

Fig. S5 Analysis of small RNAs from chrysanthemum chlorotic mottle viroid (variant CM20)-infected chrysanthemum leaves.

Fig. S6 Progeny variants from nonsymptomatic and symptomatic sectors of early, intermediate and late symptomatic leaves of chrysanthemum plants inoculated with CM20-89Umut variant.

Table S1 Primers used in this study.

Table S2 Reads of 18–26 nt obtained by high-throughput sequencing of sRNA libraries.

Table S3 Variability of the chrysanthemum chlorotic mottle viroid-sRNAs in the region containing the determinant of pathogenesis (nucleotide positions from 82 to 85).

Please note: Wiley is not responsible for the content or functionality of any Supporting Information supplied by the authors. Any queries (other than missing material) should be directed to the *New Phytologist* Central Office.